Journal of Power Sources 240 (2013) 306–313

Contents lists available at SciVerse ScienceDirect

Journal of Power Sources

journal homepage: www.elsevier.com/locate/jpowsour

Rapid carbon activation via microwave irradiation of nongraphitic carbon doped with metallic potassium and tetrahydrofuran (THF)

Sang-Eun Chun [a], J.F. Whitacre [a,b,*]

[a] Department of Materials Science and Engineering, Carnegie Mellon University, Pittsburgh, PA 15213, USA
[b] Department of Engineering and Public Policy, Carnegie Mellon University, Pittsburgh, PA 15213, USA

HIGHLIGHTS

- We demonstrate a rapid process to synthesize microporous carbon from nongraphitic carbon source through microwave-assisted exfoliation.
- While avoiding restrictive processing conditions of current chemical activation, microporous structure carbon can be efficiently synthesized.
- The specific areal capacitance reveals as high as 16.5 μF cm^{-2} in 1 M $NaNO_3$ aqueous solution.
- The electrochemical properties of the microwave-activated carbon show significant promise for use in supercapacitor electrode.

GRAPHICAL ABSTRACT

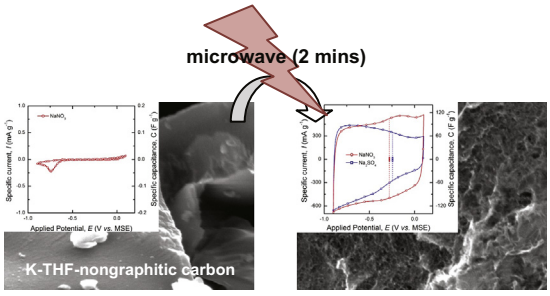

ARTICLE INFO

Article history:
Received 4 December 2012
Received in revised form
4 April 2013
Accepted 4 April 2013
Available online 11 April 2013

Keywords:
Microwave activation
Rapid activation process
Nongraphitic carbon precursor
Electrochemical capacitor
Microporous carbon
Pore shape

ABSTRACT

We report here a rapid process to synthesize microporous carbon from nongraphitic carbon source through microwave-assisted exfoliation in a non-inert environment. A ternary compound of potassium-nongraphitic carbon-tetrahydrofuran (THF) was prepared and then heating by microwave irradiation for 2 min widens the interstices between adjacent graphene layers in ternary compound, inducing microporous texture with a large amount of ultramicropores. Exploiting microwave heating allows for efficient and rapid synthesis of activated carbon compared with commonly used chemical activation process. After microwave irradiation on nongraphitic carbon, the constituent stacked graphene layers were broken and the specific surface area of 563 m^2 g^{-1} was developed. The feasibility of an electrode material for supercapacitor was estimated by cyclic voltammetry and galvanostatic charge/discharge cycling. The specific areal capacitance reveals as high as 16.4 μF cm^{-2} in 1 M $NaNO_3$ aqueous solution, which is significantly larger than values found in traditional activated carbons made for use in electrochemical double layer capacitors. Without restrictive processing conditions of chemical activation, microporous structure carbon can be efficiently and rapidly synthesized via microwave irradiation for possible electrochemical capacitor electrode.

1. Introduction

Good materials for electrochemical capacitor electrodes should have good electrical conductivity, be electrochemically stable, and have a high density of electrochemically active surface area that can interact with dissolved electrolyte species [1–3]. A variety of

* Corresponding author. Department of Materials Science and Engineering, Carnegie Mellon University, Pittsburgh, PA 15213, USA. Fax: +1 412 268 7596.
E-mail address: whitacre@andrew.cmu.edu (J.F. Whitacre).

0378-7753/$ – see front matter © 2013 Elsevier B.V. All rights reserved.
http://dx.doi.org/10.1016/j.jpowsour.2013.04.012

carbons are conductive enough for the sufficient transport of electrons for use in electronic devices. This is due to the delocalized π electrons from sp^2 hybridization bonds, which are also chemically inert [4,5]. To induce the highly porous morphology in carbonaceous materials, multiple synthetic routes and unique structures have been explored such as activation (via thermal and chemical routes) [6–11], template method [12–14], carbide-derived carbon [15,16], nanotube, fiber, aerogel, filament and so on [2]. Activation of carbon has been extensively researched [10,16]. In particular, a chemical method by using an etching agent (NaOH, KOH, H_3PO_4 and $ZnCl_2$) among versatile routes is a more aggressive process resulting in higher surface area material, but also still has a lower overall yield and more processing challenges [10].

During activation, the porosity development by an alkaline hydroxide primarily relies on the intercalation of the reduced alkali metal followed by the exfoliation and localized etching of integrated aromatic layers of precursor carbon. To drive this pore forming process, the alkali ions need to be reduced by absorbing energy at an elevated temperature. Meanwhile, a carbon material in oxygen environment easily oxidizes to form carbon monoxide or carbon dioxide above as low as 400 °C [17]. The carbon gasification (combustion) by molecular oxygen cannot contribute to develop pores due to its surface-limited reaction [10]. Hence, an inert atmosphere has to be used to avoid the removal of carbon by molecular oxygen during activation. Furthermore, the pore creation and enlargement necessitate a certain amount of processing time to achieve optimized porosity at the elevated temperature [18–20]. In brief, activation of a carbonaceous material by using alkaline hydroxide is based on the exfoliation phenomena, and the procedure using a conventional furnace requires the relatively long processing time in an inert condition at an elevated temperature to drive the process. Under this circumstance, we explore an alternative easy route to extract exfoliation phenomena from a carbonaceous material.

The exfoliation is based on the vaporization or thermal decomposition of intercalate in the graphite intercalation compound [21,22]. Alkali metal-intercalated graphite can be straightforwardly manufactured by heating a mixture of graphitic carbon and any alkali metal [23,24]. Multiple heating sources can be utilized for exfoliation such as flame, plasma, laser, microwave, electric current and so on [24]. Recently, among a wide variety of new synthesis technologies, microwave irradiation has been extensively used as a rapid and instant heating [25–29], providing the enhanced reaction rate and higher product yield. Since the sudden increase of the temperature boosts the degree of the exfoliation in the intercalation compound [21], microwave irradiation heating can be preferable for the severe exfoliation introducing large fractional pore volume. This abrupt temperature increase could provide the additional advantage of shorter processing time in contrast to conventional furnaces [30–32]. Furthermore, to avoid the previously addressed restrictive processing conditions of chemical activation, we seek to find an effective alternate way to develop highly porous nongraphitic carbon on the basis of employing microwave irradiation as a fast heating source.

Porous carbon materials obtained via chemical activation has comparably moderate areal capacitance of around 10 $\mu F\ cm^{-2}$, as compared to the high gravimetric capacitance of 100–300 $F\ g^{-1}$ [33]. Charging of capacitive material based on electric-double layer phenomena has a limiting value of 16 $\mu F\ cm^{-2}$ [34]. Understanding how to increase the areal specific capacitance to this value is of significant interest [35]. To achieve this, the dimensionality of the ionic species deployed on the electrode should be consonant with the pore dimensionality for enhanced adsorption area [36]. In this report, the feasibility of activation via the pure intercalation of an alkali metallic element followed by a microwave treatment was examined based on the variation of crystal structure, surface morphology, and electrochemical properties during non-inert process.

2. Experimental section

2.1. Material synthesis

A carbon with nongraphitic structure can be easily prepared from an organic source such as carbohydrate. In this research, nongraphitic carbon precursor was derived from the α-D-glucose (also known as dextrose, or corn syrup) (ACROS ORGANICS). To remove the initial moisture content in the as-received material, the precursor was heated at 185 °C in air atmosphere for 24 h. The produced caramelized glucose was ground into powder below 300 μm size by mesh screen. After pyrolysis under flowing N_2 of 3 $ft^3\ h^{-1}$ (1 $ft^3\ h^{-1}$ = 472 mL min^{-1}) at 500 °C, pyrolytic carbon composed of less aligned graphene layers are developed [37,38]. Since the efficient exfoliation of graphene layers can be possible in a carbon with lower ordering, the less ordered pyrolytic carbon was selected as carbon precursor.

To allow metallic potassium to intercalate into the interstices between the stacking layers, the pyrolytic carbon powder was mixed with metallic potassium previously rinsed by *n*-pentane. All experimental procedures handling potassium metal were carried out in an argon-filled glove box. Then the mixture was pyrolyzed in a horizontal tube furnace under flowing Ar gas of 3 $ft^3\ h^{-1}$ at 250 °C for 24 h. The precursor mixture was prepared by mixing the potassium and carbon in a 1:2 mass ratio. After pyrolysis, the resultant product was soaked in the tetrahydrofuran (THF) for 24 h and then sonicated for 2 h to synthesize the ternary intercalation compound of THF–potassium–carbon. THF was used to stabilize the potassium-doped graphitic carbon and operated as explosive exfoliating agent between graphene layers [30]. The resulting product was filtered and dried at 80 °C to evaporate excess THF solution under Ar gas. Subsequently, the prepared residue moved into quartz test tube was treated by microwave radiation (CEM Corporation, Discover 1) of 300 W for 2 min. The explosive reaction of the THF and potassium during the microwave irradiation involves a popping sound and sparking. The special precautions (protective equipment and fume hood) are therefore required in performing microwave activation. The final product was prepared by rinsing the sample with hot deionized water repeatedly. The resultant carbons were dried in a vacuum oven at 110 °C for 24 h. As a control experiment for microwave-assisted activation on ternary compound (THF–potassium–carbon), the nongraphitic carbon precursor was chemically activated by KOH solution agent. Various properties of the microwave-assisted activated carbon were compared with those of the KOH-activated carbon to determine the validity of the microwave activation. Nongraphitic carbon precursor was impregnated in KOH solution in a beaker for 1 h (4:1 mass ratio mixture of KOH and carbon). The precursor carbon soaked with KOH was dried at 110 °C for 12 h and then heat-treated at 800 °C in a horizontal tube furnace under a flowing Ar of 3 $ft^3\ h^{-1}$ for 2 h with a heating/cooling rate of 5 °C min^{-1}. The unreacted residual alkaline agent was rinsed by 0.5 N HCl and hot de-ionized water repeatedly until the pH of outlet water was reached 6. Finally, two sets of activated carbons were dried in a vacuum oven at 110 °C for 24 h.

2.2. Characterization

The elemental composition of the synthesized carbon was determined by elemental analysis (CE-440 Elemental Analyzer, Exeter Analytical, Inc.). The modification of surface topography via activation process was quantitatively determined by nitrogen gas

isotherm analysis (NOVA2000 series, Quantachrome Instruments). The specific surface area and pore size distribution were calculated by standard Brunauer–Emmett–Teller (BET) equation in the range of relative pressure (P/P_0) range between 0.01 and 0.21 and non-local density function theory (NLDFT), respectively. The fractional surface area contributed by each micro- and mesopores was estimated by integration of the dS/dD curve (derived from pore size distribution curve of dV/dD vs. pore width). In the pore size distribution (PSD) graph, S, V, and D are surface area, pore volume, and pore width, respectively. All experimental samples were degassed at 300 °C for 3 h prior to the measurement to remove surface contaminants and physisorbed water. Since the pyrolyzed raw carbon is composed of arrays of graphene layers, X-ray diffraction analysis (XRD) (Rigaku, Powder XRD measurement, Cu Kα) was used to estimate the crystalline structure in terms of the mass fraction of graphitically oriented graphene layers. The broad (0 0 2) Bragg peak-to-background ratio was calculated by using Matlab software. For a carbon samples reacted with potassium, XRD pattern was obtained under limited exposure condition to air.

The electrochemical properties of the synthesized carbons were measured with a multichannel potentiostat/galvanostat (VMP3, Bio-Logic) in three-electrode cell configuration, especially to discriminate the electroadsorption behavior of individual cation and anion composing electrolyte. In three electrode experimental set up with beaker type, a platinum foil as the counter electrode (CE) and mercury sulfate electrode as the reference electrode (RE) were used against working electrode (WE) containing active material. As a working electrode, the electrode consisted of well-mixed active material, binder, and conductor in an 85:10:5 mass ratios. Polytetrafluoroethylene (PTFE) (200–300 micron size) and acetylene black were used as a binder and conductor material, respectively. The electrode substance (mass: 1.5–2 mg) was pressed onto a 304 stainless steel mesh substrate using the hydraulic lab press applying approximately 50 kN. Two different aqueous solutions (1 M Na_2SO_4 and 1 M $NaNO_3$) were used as an aqueous electrolyte to observe the different electrochemical behavior of electrode materials with respect to each electrolyte. The electrochemical characteristics and performance of electrodes were analyzed by voltammetry technique (5–40 mV s^{-1}) and galvanostatic charge/discharge cycling (0.2–10 A g^{-1}). All electrochemical measurements were carried out in the potential range of 1 V (−0.9 to 0.1 V (vs. MSE)), rather narrower than 1.23 V to avoid decomposition of aqueous-based electrolyte.

3. Results/discussion

Fig. 1 illustrates the schematic procedure of microwave-assisted exfoliation of glucose-based nongraphitic carbon. A microwave irradiation technique was demonstrated as an alternate processing route to activate nongraphitic carbon precursor for the preparation of activated carbon powder. Through the prior pyrolysis of the dextrose raw material, nongraphitic carbon consisting of stacking aromatic layers was prepared. Pure potassium with carbon precursor at 250 °C for 24 h was blended for metallic potassium element to intercalate into the inner carbon structure [39]. There was no visual color change of the nongraphitic carbon sample during reaction as frequently observed in potassium-intercalated graphite with various gallery structures (K-Graphite) [23]. Upon soaking potassium-doped carbon in THF solution, the ternary compound of K–THF–carbon was synthesized. During microwave irradiation treatment of the ternary compound, sparking was evident, along with fumes and flame. The property change in the ternary compound carbon after microwave-treatment was investigated by scanning electron microscopy in an effort to probe the macroscopically porous nature of the product.

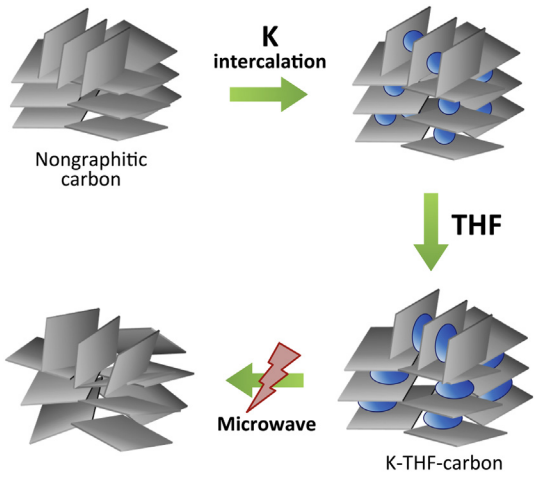

Fig. 1. Schematic illustration showing the synthesis of K–THF–carbon ternary compound and microwave-assisted exfoliation of the ternary compound.

Fig. 2(a–c) shows scanning electron micrographs of the precursor nongraphitic carbon, a K–THF–carbon ternary compound, and the resultant microwave-processed carbon, respectively. A smooth surface was formed after the pyrolysis of D-glucose. The surface of ternary compound was not modified from its original nongraphitic carbon as in Fig. 2(b). The modification by microwave resulting in an irregular surface state was observed, as a significant amount of narrow pores became evident. Through the rapid thermal decomposition/reaction of THF and intercalated metallic potassium radiated by microwave, the development of a porous structure was evolved.

The burst of potassium and THF inserted between staking layers are expected to rupture the composing graphene layers by breaking π bond energy between the layers. This rearrangement of the internal aromatic layers was examined by X-ray diffraction technique. Fig. 3 shows X-ray diffraction (XRD) patterns of the microwave-assisted activated carbon and precursor pyrolytic carbon, with XRD data of typical activated carbon by KOH solution for comparison. The patterns of the microwave-prepared carbon samples present three broad Bragg peaks consistent with the expected hexagonal (0 0 2), (1 0 0), and (1 1 0), as is commonly observed in graphitic materials with a low crystallinity. The degree of organization in the aligned graphene layers composing carbon can be quantified using the (0 0 2) peak-to-background signal ratio: 'R' value [40]. The calculated 'R' values from each sample are given in Table 1. The slightly diminished 'R' parameter observed after the process is consistent with the exfoliation of the component graphene layers which occurs during microwave treatment. Compared with this minimal change, the clear disappearance of (0 0 2) peak shown in KOH-activated carbon indicates that the stacked aromatic layers were effectively destroyed via the loss of bonding between component graphene layers during activation via alkaline solution. This comparison clearly shows that the microwave treatment is not as effective as traditional chemical etching operation in breaking the bonding energy between constituent aligned aromatic layers.

Further characterization of these porous carbon structures was carried out via BET N_2 gas adsorption technique. Fig. 4(a) shows that adsorption/desorption (isotherm) curves by N_2 gas from KOH-activated carbon and microwave-activated carbon samples. From the corresponding isotherm graphs, concurrently, the differential pore size distribution (PSD) in Fig. 4(b) was constructed by DFT theory. Microwave-activated carbon shows typical type IV isotherm with minor hysteresis, closing at the relative pressure (P/P_0) of around 0.4, indicating the presence of mesopores. The isotherm

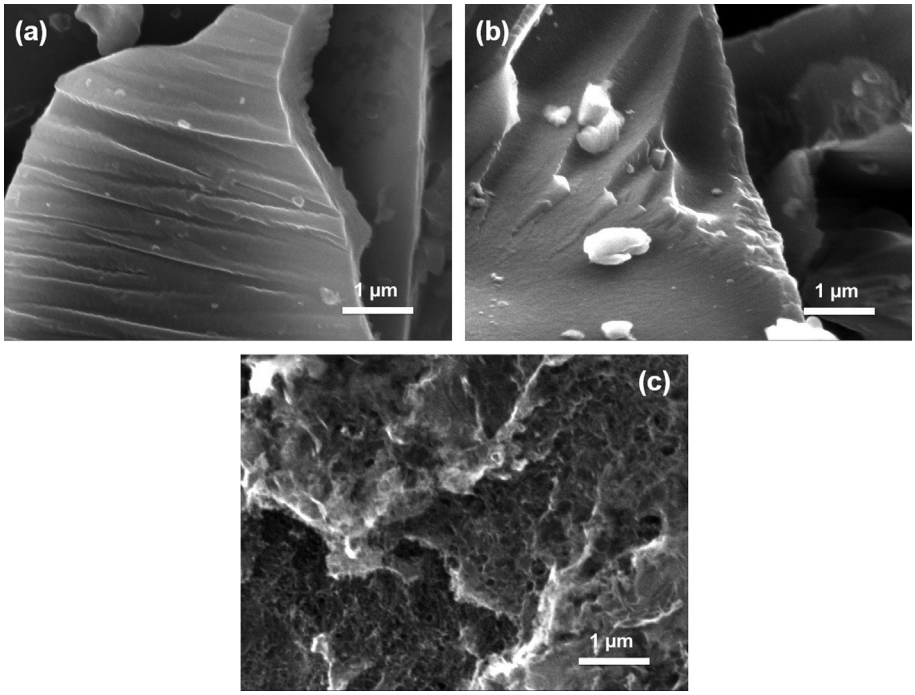

Fig. 2. SEM images during the process assisted by microwave irradiation on glucose-based carbon: (a) as-prepared carbon (pyrolyzed at 500 °C), (b) K–THF–carbon ternary compound and (c) microwave-processed carbon.

curve of KOH-activated carbon shows reversible type I isotherm exhibited in normal activated carbon with microporous texture [41]. Based on the isotherms and PSD graphs, various parameters concerning micropores or mesopores were obtained as listed in Table 2. The total pore volume in each sample was calculated from the adsorbed N_2 gas volume near unity relative pressure. In the case of pyrolytic carbon, the desorption curve does not coincide with the adsorption curve even at lowest P/P_0, indicating an irreversible uptake of N_2 [41]. For this reason, an accurate calculation of the pore distribution was not possible and was not performed here.

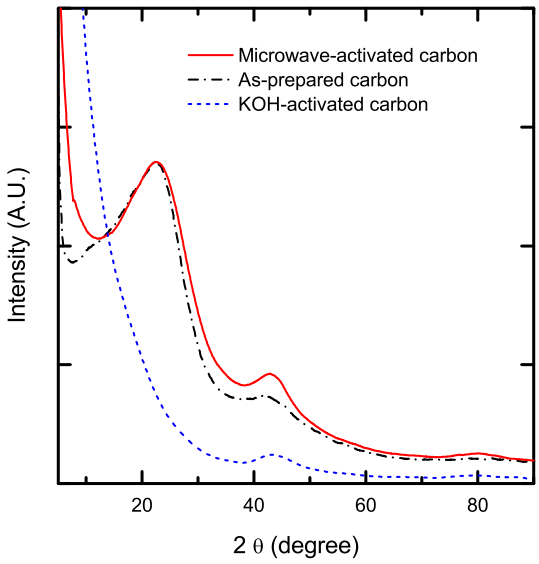

Fig. 3. X-ray diffraction patterns (XRD) measured from the nongraphitic precursor carbon before and after microwave-assisted activation process, concurrently described with XRD of chemically activated carbon by KOH solution.

Comparing the S_{BET} of two different activated carbons, approximately five times higher surface area was achieved in KOH-activated carbon compared to microwave-processed carbon. Scattering of the aligned layers by activation process possibly gave rise to fissures at the edge termination of the graphitic domains, giving diverse size ranges of pores in the graphitic layers exposed to the surface depending on the efficacy of activation. The data show that S_{BET} was less developed, and that there was a smaller volume of pores were created via microwave route.

In the PSD diagram, most of the pores in the KOH-activated carbon have dimensionalities below 2 nm. In comparison, the pores in the microwave-activated carbon gradually increase in the smaller pore width regime. In addition, due to the inherent diffusional limitation of N_2 sorption, the PSD data can only be provided in the range of above approximately 0.7 nm, and so it is possible that some of the pores had dimensionalities below this value [6]. CO_2 sorption characterization studies on this porosity effect provides the detailed morphology in the pore range of 0.4–0.8 nm [10,42].

Meanwhile, narrower pores (ultramicropore, <0.7 nm) can be efficiently characterized in an electrochemical way based on our recent research on the geometric relationship between narrow pores and electrolyte ion during electrochemical testing [36]. The data plotted in Fig. 5(a) shows cyclic voltammograms (CV) of microwave-activated carbon samples with a scanning rate of 5 mV s^{-1} in two different electrolytes: 1 mol L^{-1} Na_2SO_4 and $NaNO_3$ – electrolytes composed of a common cation (Na^+) and anions (SO_4^{2-} and NO_3^-)

Table 1
Calculated values of (0 0 2) Bragg peak-to-background ratio in X-ray diffraction graphs measured from nongraphitic carbon precursor, microwave-assisted activated carbon, and KOH-activated carbon.

	As-prepared carbon (Nongraphitic)	Microwave-assisted activated carbon	KOH-activated carbon
R value	2.20	1.81	Not measurable

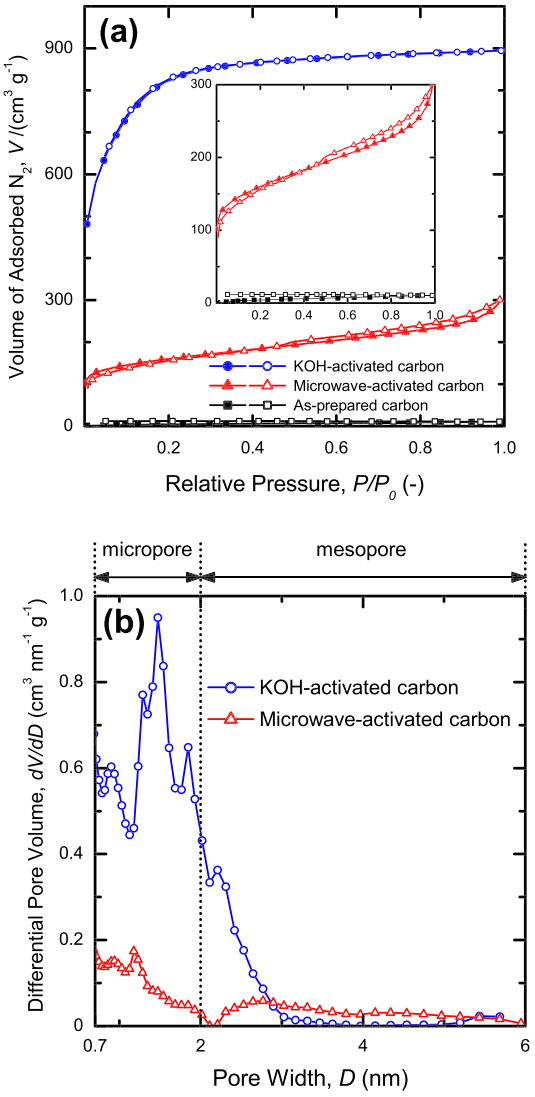

Fig. 4. (a) N_2 gas isotherm (adsorption/desorption) graph measured at 77 K (Inset illustrates the identical isotherm in an enlarged scale) and (b) corresponding pore size distribution (PSD) curve constructed based on DFT theory.

with distinctly different shapes and dimensionality. The potential of zero charge (PZC) recorded by "immersion method" [43] was marked in CV diagrams with respect to individual electrolyte. The electrokinetic experiment of CV in two distinct electrolytes was performed to characterize the porous geometry of the microwave-activated carbon, since the kinetic interaction of conducting ions with the microporous electrode is intimately associated with the geometric fitness between them [36].

Table 2
Textural parameters characterizing porous structure calculated from isotherm curves.

	Specific surface area (S_{BET})	Microporous surface area (S_{micro})	Mesoporous surface area (S_{meso})	Total pore volume
As-prepared carbon (Nongraphitic)	37 ± 1 $m^2\ g^{-1}$	Not measurable	Not measurable	0.02 $cm^3\ g^{-1}$
Microwave-activated carbon	563 ± 29 $m^2\ g^{-1}$	464 $m^2\ g^{-1}$ (86.98%)	70 $m^2\ g^{-1}$ (13.02%)	0.46 $cm^3\ g^{-1}$
KOH-activated carbon	2970 ± 154 $m^2\ g^{-1}$	2638 $m^2\ g^{-1}$ (88.83%)	332 $m^2\ g^{-1}$ (11.17%)	1.38 $cm^3\ g^{-1}$

A near-rectangular shaped CV curve was obtained when using the $NaNO_3$ electrolyte, while a declining current response was found at more cathodic potentials for the same test in the Na_2SO_4 electrolyte. This notable difference of the response current in this potential regime can be interpreted in terms of an ion sieving effect. In other words, during the potential scanning from pzc to positive vertex potential, anion species in electrolyte increasingly adsorb onto the electrode. The improved current response in $NaNO_3$ can be ascribed to the facile adsorption of the nitrate ions (NO_3^-). As anions in aqueous electrolyte, the sulfate ions (SO_4^{2-}) are electroadsorbed on an electrode in the hydrated state, while the nitrate ions (NO_3^-) are adsorbed as the nonhydrated state [44]. In addition, the effective anion size reported in the literature [44] is as follows: N_2 (3.62 Å) < NO_3^- < (4.21 Å) and (5.8 Å) < SO_2^-. Accordingly, the planar nitrate ions (NO_3^-) could be easily inserted into and adsorbed on the slit-shaped pores due to the geometric fitness of the planar electrolyte ions with the narrow pores. Hence, the expanded surface was utilized in storing the electric charge on the surface of active material, reflecting on extra capacitance of 23.52 F g^{-1} in $NaNO_3$ solution. In other words, this enhancement of surface area utilization is attributable to the favorable adsorption of NO_3^- anion alternatively used.

As shown in XRD results of microwave-activated carbon, the stacked aromatic layers were not effectively exfoliated, making deficient opening between edges of stacked graphene layers. The parted edge of layers plays a role of wall in slit-shaped pores [45,46]. Therefore, it can be assumed that more slit-like pores with narrowly open wall were developed after microwave activation. Based on the beneficial adsorption properties of NO_3^- into the slit-shaped ultramicropores, the responding current in the anion adsorption regime was noticeably enhanced for microwave-activated carbon in $NaNO_3$ solution as compared to that in the Na_2SO_4 solution.

Additionally, during anodic the scan, the small bump near −0.15 V was clearly seen in the voltammogram measured in $NaNO_3$ solution, together with faint bump around −0.3 V in Na_2SO_4. This feature probably arises from the oxidation/reduction (faradaic) reaction at the oxygen-containing carbon sites as shown in the elemental contents of Table 3 [5,47]. An additional energy storage effect was provided by this faradaic capacitance. From the voltammogram with 5 mV s^{-1}, it is revealed that microwave-activated carbon can store 92 F g^{-1} in aqueous $NaNO_3$ solution. Considering the relatively less developed surface area in microwave-activation, a notably large areal capacitance of 16.37 μF m^{-2} was achieved, which approaches the limiting areal capacitance values of the microporous activated carbon in aqueous solution [34]. In cyclic voltammograms of Fig. 5(b) and (c), the current response to the potential scanning was normalized by the active mass and the surface area, respectively. The calculated capacitance value in terms of the mass and area was summarized in Table 3. As a result, the dense electro-active surface area was achieved from the microwave activation than KOH activation, even though the higher gravimetric capacitance was obtained from KOH-activated carbon.

Since microwave-activated carbon shows enhanced electrochemical performance in $NaNO_3$ solution, the electrochemical characteristic of the sample in the same solution was also estimated with various scan rates and shown in Fig. 6. The variation of the specific capacitance was plotted depending on the operational potential based on following equation.

$$C = \frac{dQ}{dV} = \frac{I \cdot dt}{dv} = \frac{I}{dV/dt}$$

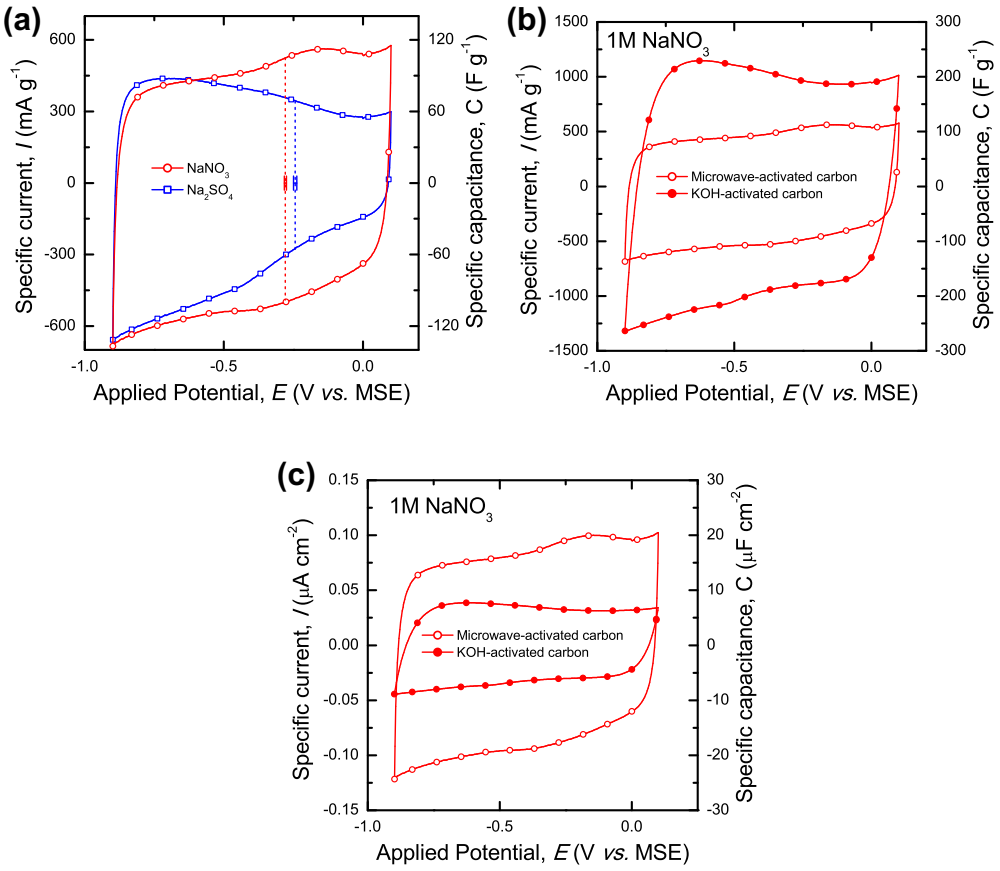

Fig. 5. (a) Cyclic voltammograms measured from microwave-assisted activated carbon with a scan rate of 5 mV s^{-1} in two sorts of electrolyte solution (1 M of Na_2SO_4 and $NaNO_3$) overlaid with vertical dotted line indicating the potential of zero charge (PZC). Cyclic voltammograms of microwave-activated carbon and KOH-activated carbon electrodes in 1 M of $NaNO_3$ with respect to (b) the active mass and (c) the surface area.

It is found that the specific capacitance decreased with the increase of the potential scan rates. Even though the nitrate ions can access the ultramicropores in the electrode, at higher scan rates the slower kinetics of ion movement into the narrower pores likely limited the availability of functional species in the relevant volumes, resulting in a decrease of the specific capacitance. In Fig. 7, the electrochemical performance of microwave-assisted activated carbon was measured with galvanostatic cycling at constant applying current of 0.2, 1.0, and 5.0 A g^{-1}. The specific capacitance was estimated to 100.7 F g^{-1}, 88.09 F g^{-1}, and 61.48 F g^{-1} at each constant current, respectively.

The fast microwave activation route of carbon shows significant promise in producing materials with very high area-normalized capacitance values. We suggest that further modification of this approach can yield materials that can compete with carbon that has been produced the more costly and time consuming chemical activation processes. Research on a large area carbonaceous electrode have led to develop the electrodes based on carbide-derived carbon (CDC) [15,48], templated porous carbon [49,50], and graphene [51,52]. Even though CDC and template method afforded the fine-tuning of pore dimension in a carbon, the difficulties in handling the sacrificial material and post-

Table 3
Elemental composition data (atomic ratio) and electrochemical performance in both activated carbon samples.

	H/C	O/C	K/C	Gravimetric capacitance	Areal capacitance
As-prepared carbon (nongraphitic)	0.57	0.11	–	0.35 F g^{-1}	0.9 μF cm^{-2}
Microwave-activated carbon	0.22	16.14	6.75	92.2 F g^{-1}	16.4 μF cm^{-2}
KOH-activated carbon	0.12	0.03	–	191.8 F g^{-1}	6.5 μF cm^{-2}

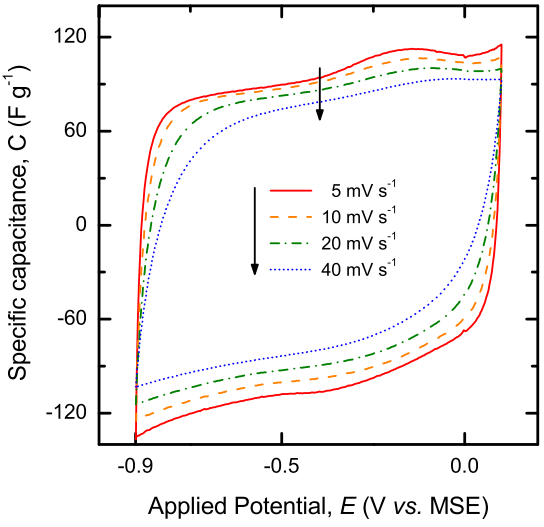

Fig. 6. Cyclic voltammograms of microwave-activated carbon sample measured at different scan rates of 5, 10, 20, and 40 mV s^{-1} in 1 M of $NaNO_3$ solution.

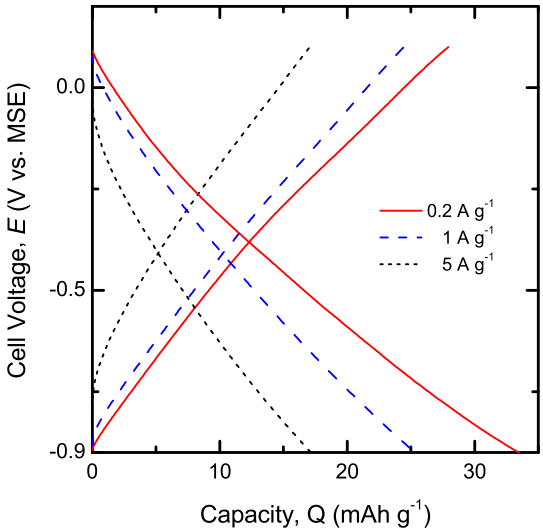

Fig. 7. Charge and discharge curve experimentally obtained by galvanostatic cycling method at three different constant current density of 0.2 A g^{-1}, 1 A g^{-1}, and 5 A g^{-1}.

processing prevent obtaining carbon in large quantities. Graphene-based electrode made from single-layer graphene with over 2630 m^2 g^{-1} necessitate the complex extraction procedure of reducing separate graphene sheet from graphene-oxide (GO) in a variety of ways [53–55]. Long processing time and inert atmosphere is the sole intricate condition for developing porous texture in chemical processing, which limitation can be avoided by using our microwave synthesis as stated. Furthermore, the fabrication via microwave irradiation displays significantly higher yield of 44 wt.% compared with the 34 wt.% in chemical activation, based on our previous report using KOH etching solution [36,38].

4. Conclusions

Microwave motivated carbon modification was carried out by exploiting intercalation of alkali metal into pyrolytic carbon, and was demonstrated as an alternate and efficient route to synthesize activated carbon from nongraphitic carbon precursor. Typical activation process via alkaline hydroxide etching only can be processed under external energy applying condition above 700 °C for a several hours. In contrast, microwave-assisted activation of nongraphitic carbon was successfully carried out based on the exfoliation of the stacking graphene layers via explosion of the inserted potassium and THF. Inert condition preventing the carbon oxidation during activation was replaced by atmospheric condition for microwave processing. Only 2 min of irradiation was needed to scatter the graphene layers of the resident nongraphitic carbon structure. As such, this processing route represents a simpler approaching to making electrochemically active materials compared to etchant-based reaction methods.

Results also showed that the developed porous structure by microwave irradiation provides unique porous texture more beneficial for the electroadsorption of nitrate ions than that of sulfate ions owing to the advantageous dimensionality of nitrate ions. Microwave treatment allowed for the rapid synthesis of activated carbon under the manageable condition, and a significantly large areal capacitance of 16.4 μF cm^{-2} in $NaNO_3$ aqueous solution compared with commercially available activated carbon, which is commonly 5–12 μF cm^{-2} [34]. Further improvement in electrochemical capacitance per mass and yield can be realized from an increment of the specific surface area by optimizing the microwave treatment process.

Acknowledgments

The authors thanks to The Department of Energy, CMU, and Aquion Energy Inc. for financial support.

References

[1] B.E. Conway, Electrochemical Supercapacitors: Scientific Fundamentals and Technological Applications, KA/PP, New York, 1999.
[2] P. Simon, Y. Gogotsi, Nat. Mater. 7 (2008) 845–854.
[3] A.G. Pandolfo, A.F. Hollenkamp, J. Power Sources 157 (2006) 11–27.
[4] F. Béguin, E. Frackowiak (Eds.), Carbons for Electrochemical Energy Storage and Conversion Systems, CRC Press, New York, 2009.
[5] K. Kinoshita, Carbon: Electrochemical and Physicochemical Properties, John Wiley and Sons, New York, 1988.
[6] F. Rodríguez-Reinosoa, A. Linares-Solano, Chemistry and Physics of Carbon, vol. 21, New York, 1988.
[7] J. Lahaye, P. Ehrburger, Fundamental Issues in Control of Carbon Gasification Reactivity, Kluwer Academic Publishers, Boston, 1991.
[8] M. Molina-Sabio, F. Rodríguez-Reinoso, F. Caturla, M.J. Sellés, Carbon 33 (1995) 1105–1113.
[9] R. Adzic, J. Zhang, K. Sasaki, M. Vukmirovic, M. Shao, J. Wang, A. Nilekar, M. Mavrikakis, J. Valerio, F. Uribe, Top. Catal. 46 (2007) 249–262.
[10] H. Marsh, F. Rodriguez-Reinoso, Activated Carbon, Elsevier, Oxford, 2006.
[11] M. Molina-Sabio, F. Rodríguez-Reinoso, Colloids Surf. A 241 (2004) 15–25.
[12] N. Sonobe, T. Kyotani, A. Tomita, Carbon 29 (1991) 61–67.
[13] R. Ryoo, S.H. Joo, S. Jun, J. Phys. Chem. B 103 (1999) 7743–7746.
[14] K. Takashi, Carbon 38 (2000) 269–286.
[15] Y. Gogotsi, A. Nikitin, H. Ye, W. Zhou, J.E. Fischer, B. Yi, H.C. Foley, M.W. Barsoum, Nat. Mater. 2 (2003) 591–594.
[16] L.R. Radovic, Chemistry and Physics of Carbon, vol. 30, CRC Press, New York, 2007.
[17] W.K. Lewis, E.R. Gilliland, R.R. Paxton, Ind. Eng. Chem. 46 (1954) 1327–1331.
[18] H. Teng, L.-Y. Hsu, Ind. Eng. Chem. Res. 38 (1999) 2947–2953.
[19] J.B. Castro, P.R. Bonelli, E.G. Cerrella, A.L. Cukierman, Ind. Eng. Chem. Res. 39 (2000) 4166–4172.
[20] Y. Lv, F. Zhang, Y. Dou, Y. Zhai, J. Wang, H. Liu, Y. Xia, B. Tu, D. Zhao, J. Mater. Chem. 22 (2012) 93–99.
[21] M. Inagaki, K. Muramatsu, Y. Maeda, K. Maekawa, Synth. Met. 8 (1983) 335–342.
[22] L.R. Radovic, Chemistry and Physics of Carbon, vol. 29, CRC Press, New York, 2007.
[23] M.S. Dresselhaus, G. Dresselhaus, Adv. Phys. 30 (1981) 139–326.
[24] D.D.L. Chung, J. Mater. Sci. 22 (1987) 4190–4198.
[25] A.V. Murugan, T. Muraliganth, A. Manthiram, Chem. Mat. 21 (2009) 5004–5006.
[26] X.-F. Guo, H. Zhan, Y.-H. Zhou, Solid State Ionics 180 (2009) 386–391.
[27] M. Zhang, D. Lei, X. Yin, L. Chen, Q. Li, Y. Wang, T. Wang, J. Mater. Chem. 20 (2010) 5538–5543.
[28] H. Yin, T. Yamamoto, Y. Wada, S. Yanagida, Mater. Chem. Phys. 83 (2004) 66–70.
[29] J.A. Gerbec, D. Magana, A. Washington, G.F. Strouse, J. Am. Chem. Soc. 127 (2005) 15791–15800.
[30] E.H.L. Falcao, R.G. Blair, J.J. Mack, L.M. Viculis, C.-W. Kwon, M. Bendikov, R.B. Kaner, B.S. Dunn, F. Wudl, Carbon 45 (2007) 1367–1369.
[31] B. Tryba, A.W. Morawski, M. Inagaki, Carbon 43 (2005) 2417–2419.
[32] O.Y. Kwon, S.W. Choi, K.W. Park, Y.B. Kwon, J. Ind. Eng. Chem. 9 (2003) 743–747.
[33] M. Inagaki, H. Konno, O. Tanaike, J. Power Sources 195 (2010) 7880–7903.
[34] J. Huang, B.G. Sumpter, V. Meunier, Chem. Eur. J. 14 (2008) 6614–6626.
[35] K. Jost, C.R. Perez, J.K. McDonough, V. Presser, M. Heon, G. Dion, Y. Gogotsi, Energy Environ. Sci. 4 (2011) 5060–5067.
[36] S.-E. Chun, J.F. Whitacre, Electrochim. Acta 60 (2012) 392–400.
[37] T. Zheng, J.S. Xue, J.R. Dahn, Chem. Mat. 8 (1996) 389–393.
[38] S.-E. Chun, Y.N. Picard, J.F. Whitacre, J. Electrochem. Soc. 158 (2011) A83–A92.
[39] L.R. Radovic, Chemistry and Physics of Carbon, vol. 29 (2004). New York.
[40] Y.H. Liu, J.S. Xue, T. Zheng, J.R. Dahn, Carbon 34 (1996) 193–200.
[41] K.S.W. Sing, D.H. Everett, R.A.W. Haul, L. Moscou, R.A. Pierotti, J. Rouquerol, T. Siemieniewska, Pure Appl. Chem. 57 (1985) 603–619.
[42] E. Raymundo-Piñero, K. Kierzek, J. Machnikowski, F. Béguin, Carbon 44 (2006) 2498–2507.
[43] M. Mülier, B. Kastening, J. Electroanal. Chem. 374 (1994) 149–158.
[44] L. Eliad, G. Salitra, A. Soffer, D. Aurbach, J. Phys. Chem. B 105 (2001) 6880–6887.
[45] J.R. Fryer, Carbon 19 (1981) 431–439.
[46] M. Huttepain, A. Oberlin, Carbon 28 (1990) 103–111.
[47] C.-T. Hsieh, H. Teng, Carbon 40 (2002) 667–674.
[48] J. Chmiola, G. Yushin, R. Dash, Y. Gogotsi, J Power Sources 158 (2006) 765–772.

[49] T. Kyotani, T. Nagai, S. Inoue, A. Tomita, Chem. Mat. 9 (1997) 609–615.
[50] T. Kyotani, Carbon 38 (2000) 269–286.
[51] M.D. Stoller, S. Park, Y. Zhu, J. An, R.S. Ruoff, Nano Lett. 8 (2008) 3498–3502.
[52] Y. Zhu, S. Murali, M.D. Stoller, K.J. Ganesh, W. Cai, P.J. Ferreira, A. Pirkle, R.M. Wallace, K.A. Cychosz, M. Thommes, D. Su, E.A. Stach, R.S. Ruoff, Science 332 (2011) 1537–1541.
[53] S. Stankovich, D.A. Dikin, G.H.B. Dommett, K.M. Kohlhaas, E.J. Zimney, E.A. Stach, R.D. Piner, S.T. Nguyen, R.S. Ruoff, Nature 442 (2006) 282–286.
[54] D. Li, M.B. Muller, S. Gilje, R.B. Kaner, G.G. Wallace, Nat. Nanotchnol. 3 (2008) 101–105.
[55] V.C. Tung, M.J. Allen, Y. Yang, R.B. Kaner, Nat. Nano 4 (2009) 25–29.